

Evidence for Bosonization in a three-dimensional gas of $SU(N)$ fermions

Bo Song,^{1,*} Yangqian Yan,^{2,*} Chengdong He,¹ Zejian Ren,¹ Qi Zhou,^{2,3,†} and Gyu-Boong Jo^{1,‡}

¹*Department of Physics, The Hong Kong University of Science and Technology,
Clear Water Bay, Kowloon, Hong Kong, China*

²*Department of Physics and Astronomy, Purdue University, West Lafayette, Indiana 47907, USA*

³*Purdue Quantum Science and Engineering Institute, Purdue University,
1205 W State St, West Lafayette, West Lafayette, IN 47907, USA*

(Dated: December 18, 2020)

Blurring the boundary between bosons and fermions lies at the heart of a wide range of intriguing quantum phenomena in multiple disciplines, ranging from condensed matter physics and atomic, molecular and optical physics to high energy physics. One such example is a multi-component Fermi gas with $SU(N)$ symmetry that is expected to behave like spinless bosons in the large N limit, where the large number of internal states weakens constraints from the Pauli exclusion principle. However, bosonization in $SU(N)$ fermions has never been established in high dimensions where exact solutions are absent. Here, we report direct evidence for bosonization in a $SU(N)$ fermionic ytterbium gas with tunable N in three dimensions (3D). We measure contacts, the central quantity controlling dilute quantum gases, from the momentum distribution, and find that the contact per spin approaches a constant with a $1/N$ scaling in the low fugacity regime consistent with our theoretical prediction. This scaling signifies the vanishing role of the fermionic statistics in thermodynamics, and allows us to verify bosonization through measuring a single physical quantity. Our work delivers a highly controllable quantum simulator to exchange the bosonic and fermionic statistics through tuning the internal degrees of freedom in any generic dimensions. It also suggests a new route towards exploring multi-component quantum systems and their underlying symmetries with contacts.

I. INTRODUCTION

Bosons and fermions exhibit intrinsically different properties because of the distinct underlying statistics. Strikingly, the boundary between bosons and fermions could become blurred under a variety of scenarios in condensed matter and high energy physics [1–4], ranging from the supersymmetry exchanging bosons and fermions [3] to fermionization of strongly interacting bosons in 1D [1, 2]. In the latter case, hardcore bosons and noninteracting fermions share identical thermodynamical properties despite the fact that their correlation functions are different [5, 6]. Another interesting route is to increase the number of spin component N in $SU(N)$ fermions leading to bosonization [7]. Theoretically, such bosonization of $SU(N)$ fermions has been extensively studied in 1D [7–14]. In this particular reduced dimension, exact solutions exist and allow one to confirm bosonization in the large N limit [7, 8]. Experimentally, this phenomenon has also been explored in 1D showing that the breathing mode of $SU(N)$ fermions approaches that of bosons with increasing N [15].

In spite of the aforementioned serious efforts of studying bosonization of $SU(N)$ fermions, some fundamental questions about bosonization of $SU(N)$ fermions remain unanswered so far. First, does bosonization of $SU(N)$ fermions occur in high dimensions? Since exact solu-

tions generically do not exist beyond 1D, it is challenging to rigorously prove the bosonization in high dimensions. In addition, the breathing mode alone cannot tell whether other thermodynamic quantities approach those of bosons. In practice, it is difficult to measure all thermodynamic quantities. Therefore, is it possible to use a single quantity to establish bosonization?

In this work, we explore bosonization of a 3D $SU(N)$ Fermi gas by measuring its central quantity, the so-called contact, \mathcal{C} [16–18] and have answered both questions. Through celebrated universal relations, contacts govern other physical observables, such as the momentum distribution, the energy, the pressure, and a variety of spectroscopies [19–24]. Therefore, the dependence of contacts on N directly provides us with the evidence of bosonization without resorting measuring other thermodynamic quantities. We choose ^{173}Yb atoms as our sample, in which the number of internal states accessible in experiments is highly tunable, ranging from one to six. Due to the strong decoupling between electronic and nuclear spins, interactions between nuclear spins are isotropic, providing the many-body system with a $SU(N)$ symmetry and consequently, a wide range of exotic phenomena [25–28].

Whereas the $SU(N)$ symmetry has been explored in optical lattices [15, 29–31], a spectroscopy [32–34], and collective excitations [15, 35], it is still challenging to measure the rather small contact due to the weak interactions between ^{173}Yb atoms. To overcome this obstacle, we develop a new protocol to extract the contact from the column integrated momentum distribution without using the inverse-Abel transform, which allows a high signal-to-noise ratio (SNR). We measure the temperature dependence of the contact when the temperature T/T_F

*These authors contributed equally to this work.

†Electronic address: zhou753@purdue.edu

‡Electronic address: gbjo@ust.hk

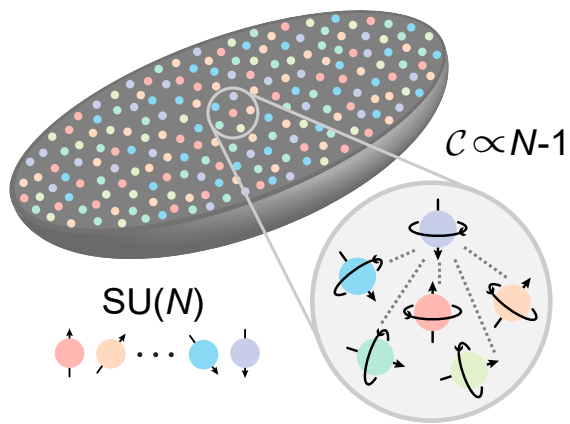


Figure 1: **Illustration of s -wave contacts in $SU(N)$ fermions with tunable spin.** Arrows with different colors and orientations denote the different nuclear spin states as large as $N=6$. Dashed lines represent pairs formed by two particles with different spins. Each pair contributes equally to the contact, which leads to $\mathcal{C} \propto N - 1$.

decreases from 1.0 to 0.55, and compare experimental results with theoretical calculations based on the virial expansion. Whereas the second order virial expansion shows a scaling of $(T/T_F)^{-3/2}$, high order virial coefficients lead to corrections from other powers of T/T_F . When N is fixed, no change in the measured contact is observed for different spin constituents, confirming the isotropic interaction. We emphasize that the underlying mechanism for $SU(N)$ fermions, the large internal degree of freedom weakening the Pauli exclusion principle, is the same for any temperatures and any interaction strengths. In different parameter regimes, the quantitative difference is how fast physical observables approach those of bosons. We thus focus on the temperature regime readily achievable in current experiments to deliver evidence for bosonization in three dimensions for the first time in laboratories, though the multi-component nature of $SU(N)$ fermions may allow a more efficient cooling down to even lower temperatures [36]. Since only a finite N is accessible in realistic experiments, it is critical to work out and experimentally verify how physical observables scale with N so as to access an unambiguous proof of bosonization in the large N limit. To this end, we further change the number of nuclear spin component N and keep the number of atoms per component constant at the same temperature and trap geometry. We find a linear dependence of the contact with N . Consequently, the contact per spin approaches a constant with a scaling law of $1 - 1/N$.

II. BOSONIZATION AND SCALING OF CONTACTS IN $SU(N)$ FERMIONS

The observed scalings of contacts can be qualitatively understood as follows. As depicted in Fig. 1, in a balanced $SU(N)$ gas with N_0 atoms per spin state, a single atom with spin- σ interacts with $(N - 1)N_0$ atoms in the other $(N - 1)$ spin components with spin- σ' ($\sigma' \neq \sigma$) through the s -wave scattering. When interactions are spin-independent, each pair of atoms contributes an equal amount, c_{pair} , to the large momentum tail, $n_{3D}^\sigma(\vec{k}) = \mathcal{C}_0/k_{3D}^4$, where $\vec{k} = (k_x, k_y, k_z)$ is a 3D momentum vector and its norm $k_{3D} = |\vec{k}|$ is much greater than k_F and other microscopic momentum scales. In the low fugacity regime where three-body correlations are negligible, $\mathcal{C}_0 = c_{\text{pair}}(N - 1)N_0^2$, i.e., scaled with $(N - 1)$ when the number of spin, N , is tuned. Correspondingly, if we consider the total momentum distribution, $n_{3D}(\vec{k}) = \sum_\sigma n_{3D}^\sigma(\vec{k})$, we could define the total contact, $\mathcal{C}_{SU(N)} = N\mathcal{C}_0 = c_{\text{pair}}N(N - 1)N_0^2$. Dividing $\mathcal{C}_{SU(N)}$ by N_t^2 , where $N_t = NN_0$ is the total particle number, we obtain that $\mathcal{C}_{SU(N)}/N_t^2 = c_{\text{pair}}(1 - 1/N)$.

In our experiment, p -wave scatterings are negligible, as the current temperature regime is smaller than the barrier of the p -wave interaction [37]. We, therefore, treat $SU(1)$ fermions as non-interacting systems. This is precisely the origin of the $1/N$ factor in the scaling of $\mathcal{C}_{SU(N)}/N_t^2$ with N . The Pauli exclusion principle suppresses the s -wave scattering between two atoms with the same spin, as well as their contributions to the s -wave contact. To make a comparison, we consider spinless bosons with the same N_t , T and the same scattering length, a_s . Though c_{pair} is independent on statistics, all $N_t(N_t - 1)/2$ pairs of particles in spinless bosons contribute to contacts such that the high momentum tail is written as $n_B(\vec{k}) = \mathcal{C}_B/k_{3D}^4$, where $\mathcal{C}_B = c_{\text{pair}}N_t(N_t - 1) \approx c_{\text{pair}}N_t^2$ for large N_0 , as the momentum distribution of identical particles doubles that of distinguishable particles. We obtain $\mathcal{C}_{SU(N)}/N_t^2 = \mathcal{C}_B/N_t^2(1 - 1/N)$, which shows that the s -wave contact of $SU(N)$ fermions approaches that of bosons with a $1/N$ scaling. Since $\mathcal{C}_0/N = (\mathcal{C}_{SU(N)}/N_t^2)N_0^2$, we use the contact per spin, \mathcal{C}_0/N , to capture this scaling with a fixed N_0 .

III. RESULTS

The experiment starts with degenerate fermions prepared in a crossed hybrid optical dipole trap (ODT) consisting of far-detuned 1064 nm and 532 nm laser light. A six-component Fermi gas of ^{173}Yb atoms, loaded from an inter-combination magneto-optical trap, is evaporatively cooled down to the temperature ~ 100 nK in the ODT in 6 s. Along with the evaporation, an arbitrary spin mixture with $N=1,2,\dots,6$ is prepared using optical pumping and blasting processes [38]. Next, we exponentially ramp

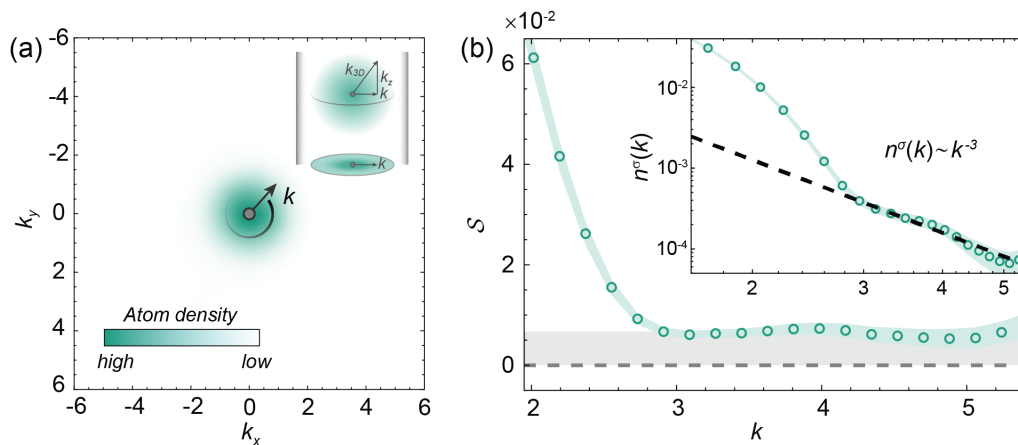


Figure 2: **Measurement of the contact parameter from the momentum distribution.** (a) Momentum distribution of ^{173}Yb atoms consisting of $N = 6$ nuclear spin states after 4 ms time-of-flight expansion. Dimensionless momentum k here is normalized by the Fermi wave number k_F . Note that momentum profile outside $k \simeq 2.5$ has already been subtracted by the momentum profile of the spin-polarised gas ($N = 1$) with the same total atom number. (b) $\mathcal{S} = 2/\pi \cdot k^3 n^\sigma(k)$ is plotted as a function of momentum k in units of k_F . Inset is the momentum tail of azimuthally averaged atomic distribution $n^\sigma(k)$ in logarithmic scale with a dashed guideline of $n^\sigma(k) \propto k^{-3}$. The $n^\sigma(k)$ is normalized as $\int n^\sigma(k) 2\pi k dk = 1$. The finite value of the contact is determined from the plateau of the \mathcal{S} profile in the range of $k = 3$ to 4. The green and grey shaded areas indicate the standard error and the measured value of contact, respectively.

up ODT to the final trap depth in 60 ms resulting in sufficiently large trap frequencies (see Appendix for details). Finally, the momentum distribution after a 4 ms time-of-flight expansion is recorded in the k_x - k_y plane by absorption imaging along the z direction using the resonant imaging light of $^1\text{S}_0 \rightarrow ^1\text{P}_1$ transition. We note that the measurement of contact at high momentum is negligibly affected by the finite expansion time [39]. In Fig. 2(b), a typical high-momentum tail is observed in the \mathcal{S} profile after the systematic noise is filtered out [40].

Our schematic protocol, for the high-precision measurement of the contact, is based on the momentum distribution of the atomic cloud after the time-of-flight expansion as shown in Fig. 2. Typically, to measure contacts from the momentum distribution, the atomic profile recorded in the 2D plane, which represents a column integrated momentum distribution, needs to be inverse-Abel transformed to a 3D momentum distribution. However, inverse-Abel transform often intensifies measurement noise and exacerbates SNR because it involves a derivative of the atomic distribution, which inevitably limits the capability to detect contacts in a weakly interacting $\text{SU}(N)$ Fermi gas. To overcome this limitation, we developed a protocol to extract contacts directly based on the weight of the high-momentum tail from a 2D time-of-flight image without using the inverse-Abel transform.

When k_{3D} is much greater than the inverse of the harmonic oscillator length and other microscopic momentum scales, $n_{3D}^\sigma(\vec{k})$ becomes isotropic in 3D and approaches \mathcal{C}_0/k_{3D}^4 . Here, we have used \mathcal{C}_0 to distinguish the original definition of contact from the scaled one, \mathcal{C} , used in our experiment. To be noted, in a spin-balanced Fermi gas with N components, atom density

for each spin $n_{3D}^\sigma(k_{3D})$ is identical. Hereafter, it is normalized such that $\int n_{3D}^\sigma(k_{3D}) d^3 k_{3D} = 1$ in our experiment. Correspondingly, the column integrated momentum distribution, $n^\sigma(k) = \int_{-\infty}^{\infty} n_{3D}^\sigma(k_{3D}) dk_z$, which follows $\int n^\sigma(k) 2\pi k dk = 1$. The momentum is normalized by the Fermi wave number $k_F = \sqrt{2E_F m}/\hbar$ with the Fermi energy $E_F = \hbar\bar{\omega}(6N_0)^{1/3}$. Here $\bar{\omega}$ is the averaged trap frequency, m is the mass of ^{173}Yb and \hbar is the reduced Planck constant. Contact \mathcal{C} can be experimentally determined from the high momentum plateau of a term $\mathcal{S} = 2/\pi \cdot k^3 n^\sigma(k)$ as follows (see Appendix),

$$\mathcal{C} = \lim_{k \rightarrow \infty} \mathcal{S}(k) = \lim_{k \rightarrow \infty} \frac{2}{\pi} \cdot k^3 n^\sigma(k) = \frac{\mathcal{C}_0}{(2\pi)^3 N_0 k_F}. \quad (1)$$

Here, \mathcal{C} is naturally normalized by the atom number per spin N_0 and the Fermi wave number k_F . The key advantage of our protocol is that no transform gets involved resulting in a high SNR ratio. To further diminish the noise of the atomic profile, we typically repeat the measurement ~ 100 times and obtain an averaged image as shown in Fig. 2(a), and then azimuthally average the momentum distribution profile with $\pm 0.2k_F$ moving average. To be noted, the value of the contact \mathcal{C} measured by our protocol is in agreement with the result extracted from the 3D momentum distribution using the inverse Abel transform as described in Appendix.

Because of the small scattering length of ^{173}Yb , contacts in our $\text{SU}(N)$ gas are contained in the large momentum tail with an extremely small amplitude that is below a thousandth of the maximum cloud density. To extract such high-momentum tail from the subtle density profile, we first filter out the systematic noise (e.g. interference fringes, imaging light fluctuation) us-

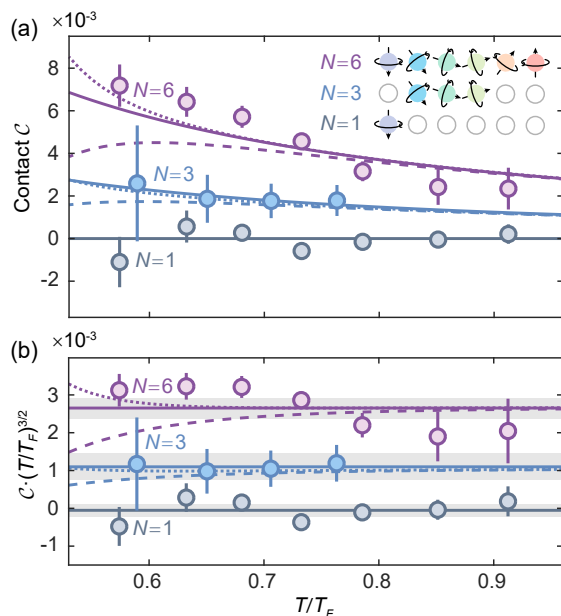


Figure 3: **Temperature scaling of contacts in SU(N) fermions.** (a) Contacts are measured at different temperatures in the SU(N) Fermi gases. The error bars represent one standard deviation in the plateau area of S profile. The solid curves are theoretical results multiplied by a factor of 7.5. Spin configuration of different SU(N) gases are presented by arrows in spheres and the circle with empty inside indicates the absence of the spin state. Details of spin configurations and preparation of different SU(N) gases are described in Appendix. Solid curves represent the results from the second order virial expansion, $C \propto (T/T_F)^{-3/2}$. Dashed and dotted curves represent results including corrections up to b_3 and b_4 , respectively. (b) Using the temperature scaling $C \propto (T/T_F)^{-3/2}$, contacts of SU(N) gases at different temperatures are collapsed to the Fermi temperature $T = T_F$. The solid line are means of collapsed contacts. The shaded grey area indicates the experimental uncertainty which consists of the standard error and the standard deviation of each point. Dashed and dotted theoretical curves including high order corrections are no longer flat. A horizontal error bar of $\pm 0.05T/T_F$ is not shown for every data point.

ing the statistical method. Our protocol is based on statistical image decomposition and projection methods using the data images as a basis set and compensating for unwanted fringes [40]. Secondly, we compare the high-momentum tail of SU($N > 1$) fermions with respect to non-interacting SU(1) gases, and extract the high-momentum tail of SU($N > 1$) gases after subtracting the counterpart of SU(1). This allows us to systematically eliminate the diffraction effect arising from atoms. Note that for a SU(1) gas, we first separate the data set of SU(1) into two parts and analyse them using a similar procedure.

In Fig. 3, we show the measured C at temperatures between $T/T_F = 0.55$ and $T/T_F = 1$ for SU($N=1,3,6$). We change the number of components, $N=1,2,\dots,6$,

but keep the same number of atoms per spin component $N_0=6.7 \times 10^3$ in a 3D harmonic trap with frequencies $(\omega_x, \omega_y, \omega_z) = 2\pi \times (1400, 750, 250)$ Hz, the averaged trap frequency $\bar{\omega} = (\omega_x \omega_y \omega_z)^{1/3} = 2\pi \times 640$ Hz and $k_F a_s \simeq 0.3$. We post-select data images according to the atom number and temperature with a tolerance of $\sim 0.1T_F$. As expected, a spin-polarized SU(1) gas with negligible p -wave scatterings does not exhibit k^4 momentum tail within our experimental uncertainty while the finite contact is clearly observed for a SU(6) or SU(3) Fermi gas in Fig. 3(a). Within the temperature regime we explored, the contact increases as the temperature T/T_F decreases.

In Fig. 4, we test the scaling of the contact with the number of the spin components in SU(N) Fermi gases. We first collapse data points in Fig. 3(a) to the Fermi temperature using $C \propto (T/T_F)^{-3/2}$ shown in Fig. 3(b). The results show that the temperature dependence of C is qualitatively consistent with the $(T/T_F)^{-3/2}$ scaling, a prediction from the second order virial expansion (Appendix). However, high order virial expansions lead to corrections to the temperature dependence of the contact, and both the third and the fourth virial coefficients, b_3 and b_4 , give rise to other powers of T/T_F in the expression of the contact (Appendix). Such corrections are plotted in both Fig. 3(a) and Fig. 3(b). Since the result from the second order virial expansion qualitatively captures temperature dependence and the current resolution in our experiment is not sufficient to accurately determine high order corrections, we empirically extract the mean values of collapsed contacts to the Fermi temperature, and further explore the dependence of the contact on N . Fig. 4(a) shows that C depends linearly on $(N-1)$, and Fig. 4(b) demonstrates that $C/N \sim C_0/N$ approaches a constant with a $1/N$ scaling. Due to the smallness of a_s/λ where $\lambda = \sqrt{2\pi\hbar^2/(mk_B T)}$ is the thermal wavelength, high order virial expansions do not change the $1/N$ scaling in the current parameter regime of our experiments (Appendix). All results are consistent with the qualitative picture we previously provided.

To measure $n^\sigma(k)$, we need to release atoms from the trap. Due to the absence of Feshbach resonance, interactions here cannot be turned off, unlike ^{40}K for studying s -wave contacts of two-component fermions [21]. Interactions lead to complex expansion dynamics that are difficult to compute in theory. Therefore, it is illuminating to theoretically study contacts of trapped gases before the expansion. We compute contacts in the temperature regime explored in the experiments, $0.55 \leq T/T_F \leq 1.0$, where the second order virial expansion works well and high order virial expansion are negligible [41, 42]. The virial expansion has been well established as a powerful tool to unfold fundamentally important principles using results at high temperatures, for instance, the universality of fermions at resonance [43, 44]. Here, the spirit is the same. The virial expansion does not only allow us to obtain quantitatively the $(1 - 1/N)$ scaling in three dimensions where exact solutions generi-

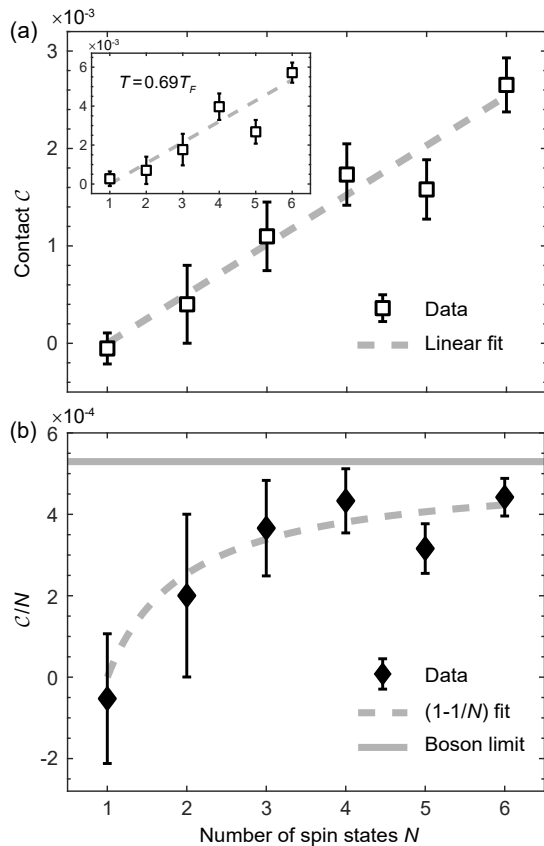


Figure 4: **Bosonization in 3D $SU(N)$ fermions.** Scaling of the contact in $SU(N)$ fermions with tunable spin is shown. (a) Contacts scale linearly with the number of spin components in a $SU(N)$ Fermi gas. Mean values of collapsed contacts at $T = T_F$ of $SU(N)$ gases are plotted as a function of number of spin states. The dashed line is a linear fit to $(N - 1)$. Inset shows contacts at $T = 0.69T_F$. (b) Contact per spin, C/N , as a function of N . The dashed line indicates a $(1-1/N)$ fit to the data. The horizontal solid line denotes the theoretical result of trapped bosons, $N_0 C_B / (8\pi^3 k_F N_t^2)$, multiplied by 7.5.

cally do not exist, but also reveal the crucial role of the large internal degree of freedom in bosonization. We evaluate the local contact at the position \vec{r} based on its local chemical potential $\mu_{loc} = \mu_0 - V(\vec{r})$, where μ_0 is the chemical potential at the center of the trap and $V(\vec{r})$ is the harmonic trapping potential. The total contact is obtained by integrating local contacts in the trap. Using the second order virial expansion, the contact is written as $C_0 = k_B T \frac{8\pi m}{\hbar^2} \left(\frac{k_B T}{\hbar\omega}\right)^3 z^2 \frac{a_s^2}{2^{3/2}\lambda} (N - 1)$. $z = e^{\beta\mu_{loc}}$ is the fugacity. In this temperature regime, the chemical potential μ_0 is well approximated by $\mu_0 = -T/T_F \cdot \log(6(T/T_F)^3) E_F$ [45]. We obtain

$$C = \frac{C_0}{(2\pi)^3 N_0 k_F} \approx \frac{m a_s^2}{6(2\pi)^{5/2} \hbar^2} \frac{E_F}{(T/T_F)^{3/2}} (N - 1). \quad (2)$$

We observe that C scales with $N - 1$ and $(T/T_F)^{-3/2}$ in the high temperature regime. In our experiments, a_s/λ

ranges between 0.06 and 0.08. In such weakly interacting regime, corrections from high order virial coefficients modify the temperature dependence but not the scaling with N (Appendix). Both scalings with T and N are consistent with the aforementioned experimental results, suggesting that interactions during the expansion do not change the scalings of the contact with T and N .

Using the virial expansion, the s -wave contact of spinless boson is also obtained explicitly in the same low fugacity regime (see Appendix). The second order virial expansion leads to

$$C_{SU(N)} = N C_0 = \left(1 - \frac{1}{N}\right) C_B. \quad (3)$$

As contact is the central quantity to control the many-body system, Eq. (3) is a direct proof of the bosonization without resorting to any other quantities, such as the full momentum distribution. Corrections from the third and the fourth virial coefficients introduce an extra temperature-dependent factor in Eq. (3) (Appendix).

Whereas scalings of the measured contacts with N and T after the expansion are consistent with theoretical results of trapped gases, experimental results lie systematically above theoretical ones, the former about 7.5 times greater than the latter (see Appendix). It is interesting to note that such discrepancy was also observed in an experiment measuring contacts of a weakly interacting Bose-Einstein condensate of ^4He atoms [46]. Interactions remain finite during expansions in both cases. It is, therefore, possible that interaction effects during the expansion lead to the aforementioned discrepancy. However, the current resolution limits our capability to measure the time dependence of contacts in the expansion, which by itself is an interesting question concerning the non-equilibrium dynamics of contacts. To avoid this issue and directly access contacts of trapped gases, an alternative scheme is the Bragg spectroscopy without the expansion [47].

IV. DISCUSSIONS AND CONCLUSION

Whereas we have focused on the high temperature regime, it will be interesting to explore the low temperature regime in the future. First, it is desirable to experimentally resolve corrections to the $1/N$ scaling, which will allow us to understand how three-body and four-body correlations may affect contacts and bosonization. Second, with further decreasing T down to below the superfluid transition temperature, our scheme of measuring contacts without using the inverse-Abel transform will provide us with an even richer playground to study contacts of superfluids with the $SU(N)$ symmetry. It has been shown that contacts of superfluids are directly related to the superfluid order parameters [48, 49]. It will be interesting to investigate how the interplay between the superfluid order and the $SU(N)$ symmetry may bring

us new macroscopic quantum phenomena and new universal relations governed by contacts, which may reveal deep connections between short-range correlations and many-body coherence.

It is worth mentioning that, due to the small scattering length of ytterbium, it is a difficult task to reach the exponentially small superfluid transition temperature. Though using other species with larger scattering lengths could increase the superfluid transition temperature, there are currently two $SU(N)$ species with $N > 2$ available in laboratories, ^{173}Yb and ^{87}Sr . Unfortunately, the latter has an even smaller a_s than ^{173}Yb we are using now. As such, a more practical approach is to implement advanced cooling schemes, such as those engineering thermal reservoirs to absorb entropy from the system of interest [50, 51]. Such schemes have been recently used to access long-range antiferromagnetic order in optical lattices [52]. It has also been recently used to access an extremely low entropy per particle of bosons down to $0.002k_b$ in optical lattices [54]. Converting such entropy to the temperatures of ideal fermions leads to $T/E_F \sim 0.0004$, a temperature scale below the superfluid transition temperature of the weakly interacting ^{173}Yb ($T/E_F \sim 0.005$ for $N = 2$). It is thus promising that superfluid transitions of $SU(N)$ fermions are accessible in the near future once the aforementioned cooling schemes or similar ones are implemented. In particular, the large spin degree of freedom may help $SU(N)$ fermions to achieve even lower temperatures than spinless bosons, due to the Pomeranchuk effect [29]. It is then expected that utilizing similar schemes in $SU(N)$ fermions will lead physicists to a new playground for exploring bosonization and many other exciting phenomena in the presence of both a large internal degree of freedom and symmetry breaking.

In addition to $SU(N)$ fermions, our high-sensitivity measurement of contact in a microscopic level is also useful for other systems. For instance, contacts has been theoretically established as a powerful tool to explore deep connections between short-range correlations and many-body physics in spin-orbit coupled systems [55–57]. Since spin-orbit coupling is the fundamental mechanism behind topological quantum matters, we hope that our works will stimulate systematic studies of contacts in topological physics.

Appendix

Preparation of $SU(N)$ gases $SU(N)$ symmetric interaction in the ground state 1S_0 of ^{173}Yb atoms emerges from the decoupling between nuclear spin and orbital angular momentum ($J = 0$). Exploiting the energy splitting of the excited state in 3P_1 to our advantage, the narrow line-width transition $^1S_0(F = 5/2) \rightarrow ^3P_1(F' = 7/2)$, with wavelength $\lambda = 556$ nm and natural line-width $\Gamma = 2\pi \times 181$ kHz, is used as a blasting light to remove unwanted m_F states of the ground

manifold 1S_0 .

The preparation starts with a gas of spin-balanced six m_F states which is initially loaded in an optical dipole trap. A sequence of short pulses of σ^\pm optical blasting light resonance to transition $m_F \rightarrow m_F \pm 1$, is applied after the end of the evaporative cooling, where the temperature of atoms is $T \sim 100$ nK. The magnetic field of 13.6 G is applied leading to a Zeeman splitting of 8.4 MHz ~ 46 Γ between two adjacent m_F states in the 3P_1 state. Take the preparation of a spin-balanced $SU(2)$ gas as an example, we shine pulses of resonant blasting light with transitions $m_F = 1/2 \rightarrow m'_F = 3/2$, $m_F = 3/2 \rightarrow m'_F = 5/2$ with σ^+ polarization to remove positive $m_F = 1/2$ and $m_F = 3/2$ respectively, and $m_F = -1/2 \rightarrow m'_F = -3/2$, $m_F = -3/2 \rightarrow m'_F = -5/2$ with σ^- polarization to remove negative $m_F = -1/2$ and $m_F = -3/2$ respectively, and the duration of each pulse is 5 ms. Following the similar method, arbitrary spin configuration of the $SU(N)$ ($N=1,2,\dots,6$) gas can be prepared by the combination of σ^+ and σ^- lights. The spin configurations of different $SU(N)$ gases used in the experiment are detected by optical Stern-Gerlach effect [38] as shown in Fig. A1.

Notably, we use optical pumping to prepare spin polarized gases ($N = 1$) with different atom numbers. At the beginning of evaporation, we first optically pump most of atoms to the $m_F = 5/2$ state using another optical pumping light 400 MHz red detuned from the resonance with $^1S_0 \rightarrow ^1P_1$ transition. The pumping pulse time is 300 ms. Note that we intentionally leave other spin states for the sake of the evaporative cooling. At the end of the evaporation, all the other remained spin states are removed by 556nm resonance light pulses similar to the procedure of $SU(N)$ gas preparation.

We further increase the trap depth to obtain large trap frequency, after the preparation of degenerate Fermi gases with different spin components at the temperature ~ 100 nK. $V(t)$, the trap depth of ODT is increased exponentially from the initial V_i to the final trap depth V_f in $t_f = 60$ ms with a time constant $\tau = 12$ ms as follows,

$$V(t) = ae^{t/\tau} + b \quad (4)$$

Where $a = (V_f - V_i)/(e^{t_f/\tau} - 1)$ and $b = V_i - a$. We have experimentally tested that T/T_F values of both non-interacting gases ($N = 1$) and weakly interacting gases ($N = 6$) are conserved during the ODT is ramped up as shown in Fig. A2.

Proof of the contact relation between \mathcal{C} and \mathcal{C}_0 Different from the original approach using the inverse Abel transform to get 3D normalized distribution $n_{3D}^\sigma(k)$ from 2D TOF image [21], the method demonstrated here is more robust against noise because the contact is directly extracted based on the radial averaged atomic distribution $n^\sigma(k)$ from 2D TOF image, illustrated in Fig.2(a) in the main text. We calculate a term $\mathcal{S} = 2/\pi \cdot k^3 n^\sigma(k)$ as a function of momentum k . The value of contact is experimentally extracted from

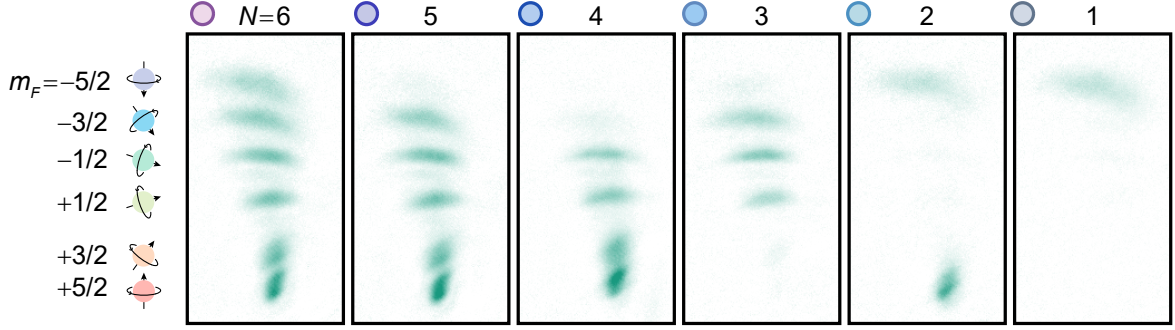


Figure A1: **Fermi gases with tunable spin components.** Unwanted spin components are removed by short pulses of resonant σ^+ and σ^- atomic transitions from $^1S_0 \rightarrow ^3P_1$ in an around 13.6 G magnetic field. From left to right, the number of spin states is prepared from $N = 6$ to $N = 1$. Optical Stern-Gerlach detection is used to monitor the spin configurations and split sub-clouds from top to bottom are $m_F = -5/2$ to $m_F = 5/2$.

the end tail of \mathcal{S} profile. The contact \mathcal{C} is therefore determined as $\mathcal{C} = \lim_{k \rightarrow \infty} \mathcal{S}$, which is slightly different from the original definition \mathcal{C}_0 [16, 17]. Contact defined here is naturally normalized by atom number per spin state N_0 and wave number k_F , and is associated with \mathcal{C}_0 as $\mathcal{C} = \mathcal{C}_0 / ((2\pi)^3 N_0 k_F)$. Here is the detail of the proof. In a spherical symmetry system which is confirmed experimentally, we start the derivation from the original definition of the contact \mathcal{C}_0 [16, 17],

$$\mathcal{C}_0 = (2\pi)^3 N_0 k_F \lim_{k_{3D} \rightarrow \infty} k_{3D}^4 n_{3D}^\sigma(k_{3D}) \quad (5)$$

Where 3D wave vector k_{3D} is normalized by k_F and 3D density $n_{3D}^\sigma(k_{3D})$ is normalized such that $\int n_{3D}^\sigma(k_{3D}) d^3 k_{3D} = 1$. The contact \mathcal{C} defined in this

article is written as,

$$\begin{aligned} \mathcal{C} &= \lim_{k \rightarrow \infty} \mathcal{S} \\ &= \lim_{k \rightarrow \infty} 2/\pi \cdot k^3 n^\sigma(k) \\ &= 2/\pi \lim_{k \rightarrow \infty} k^3 \int_{-\infty}^{\infty} n_{3D}^\sigma(k_{3D}) dk_z \end{aligned} \quad (6)$$

Here, we substitute the radial averaged atomic density with $n^\sigma(k) = \int_{-\infty}^{\infty} n_{3D}^\sigma(k_{3D}) dk_z$. From Eq. (5), for large k_{3D} , the 3D atomic density can be expressed as $n_{3D}^\sigma = \mathcal{C}_0 / ((2\pi)^3 N_0 k_F) \cdot k_{3D}^{-4} + \mathcal{O}(k_{3D}^{-5})$, in which $\mathcal{O}(k_{3D}^{-5})$ is the higher order term. Substitute n_{3D}^σ into Eq. (6), with wave vector relation $k_{3D}^2 = k^2 + k_z^2$,

$$\begin{aligned} \mathcal{C} &= \frac{2\mathcal{C}_0}{\pi(2\pi)^3 N_0 k_F} \lim_{k \rightarrow \infty} k^3 \int_{-\infty}^{\infty} \frac{dk_z}{(k^2 + k_z^2)^2} \\ &= \frac{\mathcal{C}_0}{(2\pi)^3 N_0 k_F} \end{aligned} \quad (7)$$

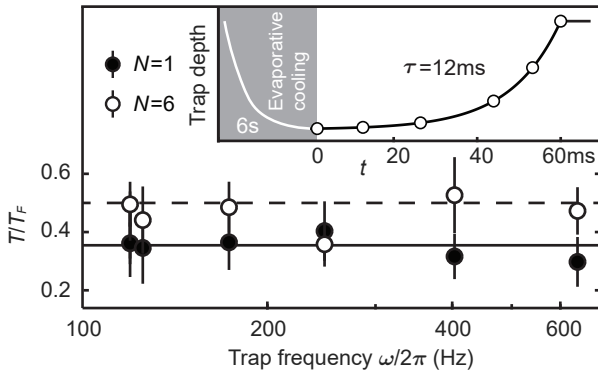


Figure A2: **The ramp-up of the optical dipole trap.** T/T_F of both non-interacting gases ($N = 1$) and weakly interacting gases ($N = 6$) are conserved during ramping up the optical dipole trap. The ODT is increased exponentially in $t_{ramp} = 60$ ms with the time constant $\tau = 12$ ms (inset). Gases with $N = 1$ and $N = 6$ components are initially prepared at $T = 0.35T_F$ and $0.5T_F$, respectively.

It is worth to note that we assume the momentum distribution is integrated over the momentum k_z in Eqs. (6,7). However, the true momentum distribution along the k_z can be slightly perturbed by atom-atom interactions during the expansion. If this is the case, the measured contact \mathcal{C} may be proportional to the equation (6) with an unknown factor. To investigate this effect, we extract the value of contact from the three-dimensional density distribution using the inverse Abel transform in Fig. A3, which does not require any approximation used in Eqs. (6,7). The contact measured from the three-dimensional density distribution is in good agreement with our result validating our detection method.

Theoretical model of contacts of SU(N) fermions In the grand-canonical ensemble, the thermodynamic potential Ω for SU(N) fermions can be expanded as a Taylor series at fugacity z (virial expansion),

$$\Omega = -k_B T Q_1(T) [Nz + N b_2^{\text{hi}} z^2 + \frac{N(N-1)}{2} b_2(T, a_s) z^2 + \dots], \quad (8)$$

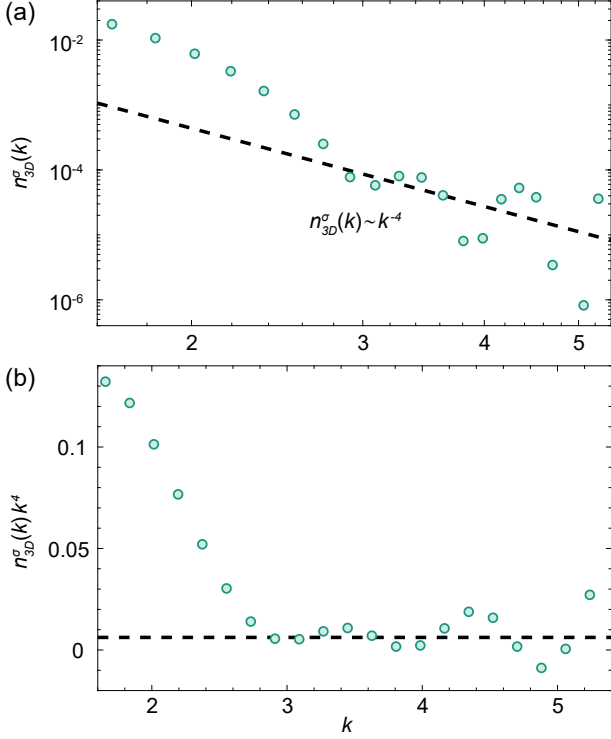


Figure A3: **Extracting the contact from the 3D momentum distribution** (a) 3D momentum distribution of a SU(6) gas is obtained from the column integrated distribution (the same data in Fig.1 in the main text) using an inverse Abel transform. The 3D density in high momentum k follows the power law $n_{3D}^\sigma(k) \sim k^{-4}$, which gives the contact $\mathcal{C} = 0.007(1)$ with 95% confidence. (b) The contact is extracted from the tail of the term $n_{3D}^\sigma(k)k^4$ for $3 < k < 4$. The mean (one standard deviation in parentheses) is $0.006(3)$. The value of the contact extracted from the 3D momentum distribution is in agreement with the result of our method $0.0067(5)$ but has a larger uncertainty.

where $Q_1(T)$ is the single particle partition function, b_2^{ni} is the intraspecies second order virial coefficient which purely arises from particle statistics, and b_2 is the interspecies second order virial coefficient which typically depends on the scattering length and temperature. Using the adiabatic relation [17],

$$\left[\frac{\partial \Omega}{\partial a_s^{-1}} \right]_{T, \mu} = \frac{\hbar^2 N}{8\pi m} \mathcal{C}_0, \quad (9)$$

we obtain an virial expansion of the contact from Ref. [53],

$$\mathcal{C}_0 = k_B T \frac{4\pi m}{\hbar^2} Q_1(T) z^2 \frac{\partial b_2(T, a_s)}{\partial a_s^{-1}} (N-1). \quad (10)$$

Comparing the Taylor expansion of the grand canonical potential Ω with the virial coefficient, we obtain

$$b_2(a_s, T) = Q_{1,1}/Q_1, \quad (11)$$

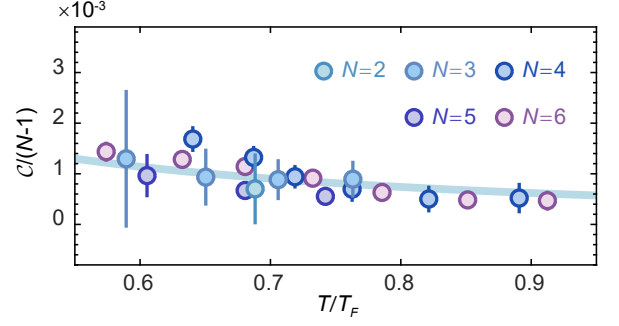


Figure A4: **Scaled contact vs temperature** Contact of different SU(N) gases are scaled on the $N = 2$ components case by $\mathcal{C}/(N-1)$. The solid curve is the theoretical simulation multiplied by a factor of 7.5.

where $Q_{1,1}$ is the partition function of two particles of different species in the anisotropic trap. According to Ref. [58], one could transform the problem, to a very good approximation at high temperature, to a spherical harmonic trap with trapping frequency $\bar{\omega}$ satisfies

$$3\bar{\omega}^2 = \omega_x^2 + \omega_y^2 + \omega_z^2. \quad (12)$$

Using the energy spectrum of two particles under isotropic harmonic confinement at any scattering length obtained from solutions in Ref. [59] we can numerically determine the partition function as well as the derivative with respect to a_s^{-1} .

According to local density approximation, at high temperature where $k_B T \gg \hbar \bar{\omega}$, the virial coefficient for the trapped system can be related to that of the homogeneous system.

$$b_2 \approx b_2^{\text{homo}}/2^{3/2}, \quad (13)$$

$$Q_1 \approx (k_B T/\hbar \bar{\omega})^3, \quad (14)$$

where $\bar{\omega}^3 = \omega_x \omega_y \omega_z$. From Ref. [43], one obtain $b_2^{\text{homo}} = -2a_s/\lambda$, where λ is the thermal de Broglie length. Combining the equations above, under LDA, we obtain

$$\mathcal{C}_0 = k_B T \frac{4\pi m}{\hbar^2} (k_B T/\hbar \bar{\omega})^3 z^2 \frac{2a_s^2}{2^{3/2}\lambda} (N-1). \quad (15)$$

In the high temperature limit, $z = N_0(\hbar \bar{\omega}/k_B T)^3$. The total contact of SU(N) fermions is then written as

$$\mathcal{C}_{\text{SU}(N)} = N\mathcal{C}_0 = N_0^2 N(N-1) \frac{2\sqrt{2}\pi m}{\hbar^2} \frac{(\hbar \bar{\omega})^3}{(k_B T)^2} \frac{a_s^2}{\lambda}. \quad (16)$$

Contact of single component Bose gas Applying the virial expansion to a single-component Bose gas, the thermodynamic potential Ω_B at high temperatures is written as

$$\Omega_B = -k_B T Q_1(T) [z_B + b_2^{\text{niB}} z_B^2 + b_2(T, a_s) z_B^2 + \dots]. \quad (17)$$

Here b_2 is the second order virial coefficient for two distinguishable particles, i.e., the same as that for the intraspecies b_2 for SU(N) fermions, and b_2^{niB} is a term that accounts for bosonic statistics which is independent of the scattering length. Using the adiabatic relation [17],

$$\left[\frac{\partial \Omega_B}{-a_s^{-1}} \right]_{T,\mu} = \frac{\hbar^2}{8\pi m} \mathcal{C}_B, \quad (18)$$

we obtain an virial expansion of the contact,

$$\mathcal{C}_B = k_B T \frac{8\pi m}{\hbar^2} Q_1(T) z^2 \frac{\partial b_2(T, a_s)}{\partial a_s^{-1}}. \quad (19)$$

Using $z_B = NN_0(\hbar\bar{\omega}/k_B T)^3$, we obtain

$$\mathcal{C}_B = (N_0 N)^2 \frac{2\sqrt{2}\pi m}{\hbar^2} \frac{(\hbar\bar{\omega})^3}{(k_B T)^2} \frac{a_s^2}{\lambda}. \quad (20)$$

Compare \mathcal{C}_B and $\mathcal{C}_{\text{SU}(N)}$, we obtain

$$\mathcal{C}_{\text{SU}(N)} = \frac{N-1}{N} \mathcal{C}_B. \quad (21)$$

In the limit $N \rightarrow \infty$, $\mathcal{C}_{\text{SU}(N)}$ approaches \mathcal{C}_B with a scaling of $1/N$.

High order virial expansions With decreasing temperature, high order virial expansions are required. We consider corrections up to b_4 , i.e.,

$$\Omega = -k_B T Q_1(T) [Nz + Nb_2^{\text{ni}} z^2 + \frac{N(N-1)}{2} b_2(T, a_s) z^2] - k_B T (\Omega_3 z^3 + \Omega_4 z^4 \dots), \quad (22)$$

where

$$\Omega_3 = \binom{N}{3} Q_{1,1,1} + 2 \binom{N}{2} Q_{1,2} + N Q_3 - N Q_1 \left(N Q_2 + \binom{N}{2} Q_{1,1} \right) + N^3 Q_1^3 / 3 \quad (23)$$

$$\begin{aligned} \Omega_4 = & N(N-1) Q_{1,3} + \binom{N}{2} Q_{2,2} + \binom{N-1}{2} N Q_{1,1,2} \\ & + \binom{N}{4} Q_{1,1,1,1} + N Q_4 \quad (24) \\ & - N Q_1 \left(\binom{N}{3} Q_{1,1,1} + N Q_3 + N(N-1) Q_{1,2} \right) \\ & - \frac{1}{2} \left(\binom{N}{2} Q_{1,1} + N Q_2 - N^2 Q_1^2 \right)^2 + \frac{1}{2} N^4 Q_1^4; \end{aligned}$$

Here, $\binom{N}{k} = N!/(k!(N-k)!)$ is the binomial coefficient, Q_{n_1, n_2, \dots, n_N} means the partition function of the N -component fermionic system with n_i number of fermions in the i th component and the order of n_1, n_2, \dots, n_N does not matter because all spins are equivalent. For instance, $Q_{1,2}$ means the partition function of three fermions with one particle in one spin state and two particles in another one. When each of the three fermions occupies a different spin state, its partition function is denoted by $Q_{1,1,1}$.

In our experiment, a_s/λ is a small number between 0.06 and 0.08. In such a weakly interaction regime, where $(a_s/\lambda)^2 \ll 1$, $Q_{1,1,1} = Q_1^3 + 3(Q_{1,1} - Q_1^2)Q_1 + O((a_s/\lambda)^2)$. This result can be understood from the fact that the partition function of three fermions, all of which occupy different spin states, reduces to Q_1^3 in the non-interacting limit. Turning on a weak interaction, the leading correction is $3(Q_{1,1} - Q_1^2)Q_1 \sim a_s/\lambda$, i.e, these three fermions can be decomposed to a pair of particles, which are interacting with the two-body interaction, and a remaining one that does not interact with the pair. The factor of 3 comes from the three ways of such decomposition. We thus obtain

$$\begin{aligned} \Omega_3 = & 2 \binom{N}{2} (Q_{1,2} - Q_1 Q_2 - Q_{1,1} Q_1 + Q_1^3) \quad (25) \\ & + N (Q_3 - Q_1 Q_2 + Q_1^3 / 3). \end{aligned}$$

Similar to what we have seen in the second order virial expansion, Ω_3 can also be separated into two parts, one is the result of non-interacting systems, and other other is the correction from interactions. We thus rewrite the above equation as

$$\Omega_3 / Q_1 = N(N-1) b_3^{\text{int}} + N b_3^{\text{ni}}, \quad (26)$$

where $b_3^{\text{int}} \equiv (Q_{1,2} - Q_1 Q_2 - Q_{1,1} Q_1 + Q_1^3) / Q_1$ and $b_3^{\text{ni}} \equiv (Q_3 - Q_1 Q_2 + Q_1^3 / 3) / Q_1$. Again, the non-interacting part of b_3 is proportional to N , while the contribution from interactions is proportional to $N(N-1)$. Higher powers of N , such as $N(N-1)(N-2)$, which is at least of the order of $(a_s/\lambda)^2$, are high order corrections and thus are negligible in the weakly interacting regime.

The same analyses can be applied to b_4 . In the weakly interacting regime, $a_s/\lambda \ll 1$, the partition functions of more than 3 spin components can be expressed in terms of those of two and one spin components. We thus obtain

$$\begin{aligned} -\frac{\Omega}{N k_B T Q_1} = & z + \frac{1}{2} z^2 ((N-1) b_2^{\text{int}} + b_2^{\text{ni}}) \quad (27) \\ & + \frac{1}{3} z^3 (3(N-1) b_3^{\text{int}} + b_3^{\text{ni}}) \\ & + \frac{1}{4} z^4 (4(N-1) b_4^{\text{int}} + b_4^{\text{ni}}) + \dots \end{aligned}$$

where, b_n are expanded in terms of a_s/λ ,

$$b_2^{\text{ni}} = -1/8, \quad (28)$$

$$b_2^{\text{int}} = -\frac{a_s}{\sqrt{2}\lambda} + O\left(\frac{a_s}{\lambda}\right)^2, \quad (29)$$

$$b_3^{\text{ni}} = 1/27, \quad (30)$$

$$b_3^{\text{int}} = \frac{a_s}{3\sqrt{6}\lambda} + O\left(\frac{a_s}{\lambda}\right)^2, \quad (31)$$

$$b_4^{\text{ni}} = -1/64, \quad (32)$$

$$b_4^{\text{int}} = -\left(\frac{1}{64} + \frac{1}{12\sqrt{3}}\right) \frac{a_s}{\lambda} + O\left(\frac{a_s}{\lambda}\right)^2. \quad (33)$$

To derive these expressions, we have adopted the results of SU(2) Fermi gas, i.e., $Q_{1,2}$, $Q_{1,3}$, etc. [60]. As

expected, the dimensionless b_n must be power series of the dimensionless parameter a_s/λ . Using Ω , we obtain both the total particle number and the contact,

$$NN_0 = -\frac{\partial\Omega}{\partial\mu} = -\frac{\partial\Omega}{\partial z} \frac{\partial z}{\partial\mu} = -\frac{\partial\Omega}{\partial z} \frac{z}{k_B T}, \quad (34)$$

$$\frac{N\hbar^2}{8\pi m} \mathcal{C}_0 = -\frac{\partial\Omega}{\partial a_s^{-1}}, \quad (35)$$

both of which can be expressed in power series of z . Eliminating z , we obtain the contact as a function of N , N_0 , and T ,

$$\mathcal{C}_0^{(4)} = \mathcal{C}_0^{(2)} f_F\left(\frac{T}{T_F}; k_F a_s\right) \quad (36)$$

$$\begin{aligned} f_F\left(\frac{T}{T_F}; k_F a_s\right) = & \left[1 - \left(\frac{1}{9\sqrt{3}} - \frac{1}{48}\right)(T/T_F)^{-3} \right. \\ & + \left(\frac{1}{108\sqrt{6}} + \frac{1}{576\sqrt{2}} - \frac{5}{31104} - \frac{1}{216\sqrt{3}}\right)(T/T_F)^{-6} \\ & + \frac{(N-1)k_F a_s}{12\sqrt{2\pi}}(T/T_F)^{-5/2} + 2\left(\frac{(N-1)k_F a_s}{12\sqrt{2\pi}}\right)^2(T/T_F)^{-5} \\ & \left. - (N-1)\frac{k_F a_s}{2\sqrt{\pi}}\left(\frac{7}{108\sqrt{6}} - \frac{1}{72\sqrt{2}}\right)(T/T_F)^{-11/2} + \dots \right] \end{aligned} \quad (37)$$

which is accurate up to $(T/T_F)^{-6}$. This requires us to include contributions up to b_4 in Eq. (35) and up to b_3 in Eq. (34). Here, the Fermi temperature is a function of N_0 , $T_F = \hbar\bar{\omega}(6N_0)^{1/3}/k_B$, a_s/λ is replaced by $\frac{k_F a_s}{2\sqrt{\pi}}\sqrt{T/T_F}$. $\mathcal{C}_0^{(2)}$ is the previously obtained contact in the second order virial expansion, as shown in Eq. (15). Since $\mathcal{C}_0^{(2)} \sim (N-1)$, the last three terms in the above equation leads to higher powers of N in the scalings of the contact with N . However, all of them are much smaller than the other terms due to the smallness of $k_F a_s$ and a_s/λ . Using our experimental parameters, the total correction from these $(N-1)$ -dependent terms for $N=6$ is up to 13%, 10%, 5% for $T/T_F = 0.55, 0.69$, and 1 respectively. Thus, $\mathcal{C} = \frac{\mathcal{C}_0}{(2\pi)^3 N_0 k_F}$ scales with $(N-1)$ in our experiments.

The slope of the linear scaling of \mathcal{C} with $N-1$ is temperature dependent. Theoretical results plotted in Fig. A5 show that the slope increases with decreasing T . This has also been observed in experiments. As shown in Fig. 3(b), our experimental resolution is not able to distinguish the small curvatures, which come from the small high order corrections to the linear scaling of \mathcal{C} with $N-1$. As such, we use a linear fitting to obtain the slope. Again, the theoretical results of the slope are about 6-9 times of the experimentally observed ones due to the expansion dynamics, as explained in the main text.

If we only keep contributions up to b_3 in Eq. (35) and b_2 in Eq. (34),

$$\begin{aligned} \mathcal{C}_0^{(3)} = \mathcal{C}_0^{(2)} & \left[1 - \left(\frac{1}{9\sqrt{3}} - \frac{1}{48}\right)(T/T_F)^{-3} \right. \\ & \left. + \frac{(N-1)k_F a_s}{12\sqrt{2\pi}}(T/T_F)^{-5/2} + \dots \right] \end{aligned} \quad (38)$$

Both results have been presented in Fig. 3 of the main text.

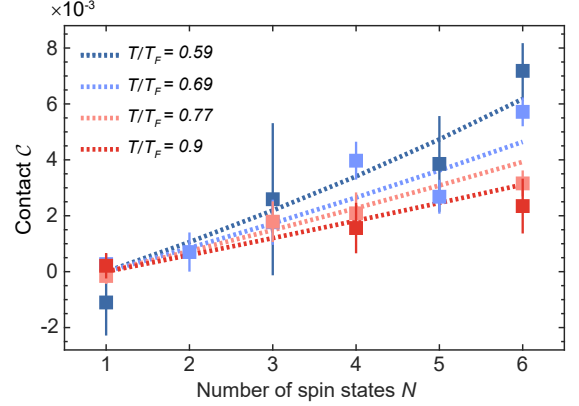


Figure A5: Contact as a function of spin component N at different temperatures T/T_F . Experimental results are denoted by boxes. Dotted lines represent theoretical results including corrections up to fourth order virial expansion. All theoretical curves have included a factor of 7.5.

High order virial expansions for bosons The above analysis can be applied to bosons as well.

$$\mathcal{C}_B^{(4)} = \mathcal{C}_B^{(2)} f_B\left(\frac{T}{T_F}; k_F a_s\right), \quad (39)$$

$$\begin{aligned} f_B\left(\frac{T}{T_F}; k_F a_s\right) = & \left[1 + \left(\frac{1}{9\sqrt{3}} - \frac{1}{48}\right)N(T/T_F)^{-3} \right. \\ & + \left(\frac{1}{108\sqrt{6}} + \frac{1}{576\sqrt{2}} - \frac{5}{31104} - \frac{1}{216\sqrt{3}}\right)N^2(T/T_F)^{-6} \\ & + \frac{k_F a_s}{6\sqrt{2\pi}}N^{5/6}(T/T_F)^{-5/2} + \frac{(k_F a_s)^2}{36\pi}N^{5/3}(T/T_F)^{-5} \\ & \left. + \left(\frac{7}{54\sqrt{6}} - \frac{1}{36\sqrt{2}}\right)\frac{k_F a_s}{2\sqrt{\pi}}N^{11/6}(T/T_F)^{-11/2} \dots \right] \end{aligned} \quad (40)$$

Here, $\mathcal{C}_B^{(2)}$ is the previously obtained contact of bosons in the second order virial expansion, as shown in Eq. (20). T_F is defined to be the Fermi temperature of the corresponding Fermi gas of a single component, $T_F = \hbar\bar{\omega}(6N_0)^{1/3}/k_B$, for convenience of comparison. Using the results of both bosons and SU(N) fermions, we obtain

$$\mathcal{C}_{\text{SU}(N)}^{(4)} = N\mathcal{C}_0^{(4)} = \alpha\left(\frac{T}{T_F}; k_F a_s\right)\left(1 - \frac{1}{N}\right)\mathcal{C}_B^{(4)}, \quad (41)$$

where $\alpha\left(\frac{T}{T_F}; k_F a_s\right) = \frac{f_B(T/T_F; k_F a_s)}{f_F(T/T_F; k_F a_s)}$. The virial expansion works for SU(N) fermions and bosons in the temperature regimes $T \gtrsim 0.55T_F$ and $T \gtrsim 0.55N^{1/3}T_F$, respectively. At $T \gg 0.55N^{1/3}T_F$, both $f_F\left(\frac{T}{T_F}; k_F a_s\right)$ and $f_B\left(\frac{T}{T_F}; k_F a_s\right)$ can be well approximated by 1. As such, $\mathcal{C}_{\text{SU}(N)}^{(4)} \rightarrow \mathcal{C}_B^{(4)}$ when $N \rightarrow \infty$.

-
- [1] S. Weinberg, *The Quantum Theory of Fields* (University of Texas, Austin, 2000).
- [2] T. Giamarchi, *Quantum Physics in One Dimension* (Clarendon Press, Oxford, 2003).
- [3] Z. X. Li, A. Vaezi, C. B. Mendl and H. Yao, *Numerical observation of emergent spacetime supersymmetry at quantum criticality*, Science Advances **4**, eaau1463 (2018).
- [4] A. Cherman and D. Dorigoni, *Large N and bosonization in three dimensions*, Journal of High Energy Physics **2012**, 173 (2012).
- [5] B. Paredes, A. Widera, V. Murg, O. Mandel, S. Fölling, I. Cirac, G. V. Shlyapnikov, T. W. Hänsch, and I. Bloch, *Tonks-Girardeau gas of ultracold atoms in an optical lattice*, Nature **429**, 277 (2004).
- [6] T. Kinoshita, T. Wenger, and D. S. Weiss, *Observation of a One-Dimensional Tonks-Girardeau Gas*, Science **305**, 1125 (2004).
- [7] C. N. Yang and Y.-Z. You, *One-Dimensional w -Component Fermions and Bosons with Repulsive Delta Function Interaction*, Chinese Physics Letters **28**, 020503 (2011).
- [8] X.-W. Guan, Z.-Q. Ma and B. Wilson, *One-dimensional multicomponent fermions with δ -function interaction in strong- and weak-coupling limits: κ -component Fermi gas*, Phys. Rev. A **85**, 033633 (2012).
- [9] Xia-Ji Liu and Hui Hu, *Collective mode evidence of high-spin bosonization in a trapped one-dimensional atomic Fermi gas with tunable spin*, Annals of Physics **350** 84-94 (2014).
- [10] Yuzhu Jiang, Peng He and Xi-Wen Guan, *Universal low-energy physics in 1D strongly repulsive multi-component Fermi gases*, Journal of Physics A: Mathematical and Theoretical **49** 17 (2016).
- [11] Jen, H. H. and Yip, S.-K., *Spin-incoherent Luttinger liquid of one-dimensional $SU(\kappa)$ fermions*, Phys. Rev. A **98** 013623 (2018).
- [12] Xi-Wen Guan, Murray T. Batchelor, and Chaohong Lee, *Fermi gases in one dimension: From Bethe ansatz to experiments*, Rev. Mod. Phys. **85**, 1633 (2013).
- [13] Jean Decamp, Johannes Jünemann, Mathias Albert, Matteo Rizzi, Anna Minguzzi, and Patrizia Vignolo, *High-momentum tails as magnetic-structure probes for strongly correlated $SU(\kappa)$ fermionic mixtures in one-dimensional traps*, Phys. Rev. A **94**, 053614 (2016).
- [14] E. K. Laird, Z.-Y. Shi, M. M. Parish, and J. Levinsen, *$SU(N)$ fermions in a one-dimensional harmonic trap*, Phys. Rev. A **96**, 032701 (2017).
- [15] G. Pagano, M. Mancini, G. Cappellini, P. Lombardi, F. Schäfer, H. Hu, X.-J. Liu, J. Catani, C. Sias, M. Inguscio et al., *A one-dimensional liquid of fermions with tunable spin*, Nature Physics **10**, 198 (2014).
- [16] S. Tan, *Energetics of a strongly correlated Fermi gas*, Annals of Physics **323**, 2952 (2008).
- [17] S. Tan, *Large momentum part of a strongly correlated Fermi gas*, Annals of Physics **323**, 2971 (2008).
- [18] S. Tan, *Generalized virial theorem and pressure relation for a strongly correlated Fermi gas*, Annals of Physics **323**, 2987 (2008).
- [19] G. B. Partridge, K. E. Strecker, R. I. Kamar, M. W. Jack, and R. G. Hulet, *Molecular Probe of Pairing in the BEC-BCS Crossover*, Phys. Rev. Lett. **95**, 020404 (2005).
- [20] F. Werner, L. Tarruell, and Y. Castin, *Number of closed-channel molecules in the BEC-BCS crossover*, The European Physical Journal B **68**, 401 (2009).
- [21] J. T. Stewart, J. P. Gaebler, T. E. Drake and D. S. Jin, *Verification of Universal Relations in a Strongly Interacting Fermi Gas*, Phys. Rev. Lett. **104**, 235301 (2010).
- [22] E. Kuhnle, S. Hoinka, P. Dyke, H. Hu, P. Hannaford, and C. Vale, *Crossover from 2D to 3D in a Weakly Interacting Fermi Gas*, Phys. Rev. Lett. **106**, 170402 (2011).
- [23] R. J. Fletcher, R. Lopes, J. Man, N. Navon, R. P. Smith, M. W. Zwierlein, and Z. Hadzibabic, *Two- and three-body contacts in the unitary Bose gas*, Science **355**, 377 (2017).
- [24] S. Laurent, M. Pierce, M. Delehaye, T. Yefsah, F. Chevy, and C. Salomon, *Connecting Few-Body Inelastic Decay to Quantum Correlations in a Many-Body System: A Weakly Coupled Impurity in a Resonant Fermi Gas*, Phys. Rev. Lett. **118** (2017).
- [25] C. Wu, J.-p. Hu and S.-C. Zhang, *Exact $SO(5)$ Symmetry in the Spin-3/2 Fermionic System*, Phys. Rev. Lett. **91**, 186402 (2003).
- [26] M. Hermele, V. Gurarie and A. Rey, *Mott Insulators of Ultracold Fermionic Alkaline Earth Atoms: Underconstrained Magnetism and Chiral Spin Liquid*, Phys. Rev. Lett. **103**, 135301 (2009).
- [27] A. V. Gorshkov, M. Hermele, V. Gurarie, C. Xu, P. S. Julienne, J. Ye, P. Zoller, E. Demler, M. D. Lukin and A. M. Rey, *Two-orbital $SU(N)$ magnetism with ultracold alkaline-earth atoms*, Nature Physics **6**, 289 (2010).
- [28] M. A. Cazalilla and A. M. Rey, *Ultracold fermi gases with emergent $SU(N)$ symmetry*, Reports on Progress in Physics **77**, 124401 (2014).
- [29] S. Taie, R. Yamazaki, S. Sugawa and Y. Takahashi, *An $SU(6)$ Mott insulator of an atomic Fermi gas realized by large-spin Pomeranchuk cooling*, Nature Physics **8**, 825 (2012).
- [30] C. Hofrichter, L. Riegger, F. Scazza, M. Höfer, D. R. Fernandes, I. Bloch and S. Fölling, *Direct Probing of the Mott Crossover in the $SU(N)$ Fermi-Hubbard Model*, Phys. Rev. X **6**, 021030 (2016).
- [31] H. Ozawa, S. Taie, Y. Takasu and Y. Takahashi, *Antiferromagnetic Spin Correlation of $SU(N)$ Fermi Gas in an Optical Superlattice*, Phys. Rev. Lett. **121**, 225303 (2018).
- [32] X. Zhang, M. Bishof, S. L. Bromley, C. V. Kraus, M. S. Safronova, P. Zoller, A. M. Rey and J. Ye, *Spectroscopic observation of $SU(N)$ -symmetric interactions in Sr orbital magnetism*, Science **345**, 1467 (2014).
- [33] G. Cappellini, M. Mancini, G. Pagano, P. Lombardi, L. Livi, M. Siciliani de Cumis, P. Cancio, M. Pizzocaro, D. Calonico, F. Levi, C. Sias, J. Catani, M. Inguscio, and L. Fallani, *Direct observation of coherent interorbital spin-exchange dynamics*, Phys. Rev. Lett. **113**, 120402 (2014).
- [34] F. Scazza, C. Hofrichter, M. Hofer, P. C. De Groot, I. Bloch and S. Fölling, *Observation of an Orbital Interaction-Induced Feshbach Resonance in Yb 173*, Nature Physics **11**, 514 (2015).
- [35] C. He, Z. Ren, B. Song, E. Zhao, J. Lee, Y.-C. Zhang, S. Zhang and G.-B. Jo, *Collective excitations in two-dimensional $SU(N)$ Fermi gases with tunable spin*, Phys. Rev. Research **2** 012028(R) (2020).

- [36] L. Sonderhouse, C. Sanner, R. B. Hutson, A. Goban, T. Bilitewski, L. Yan, W. R. Milner, A. Maria Rey, and J. Ye, *Thermodynamics of a deeply degenerate $SU(N)$ -symmetric Fermi gas*, Nature Physics (2020) <https://doi.org/10.1038/s41567-020-0986-6>.
- [37] T. Fukuhara, Y. Takasu, M. Kumakura and Y. Takahashi, *Degenerate Fermi gases of ytterbium*, Phys. Rev. Lett. **98**, 030401 (2007).
- [38] B. Song, C. He, S. Zhang, E. Hajiyev, W. Huang, X.-J. Liu and G.-B. Jo, *Spin-orbit-coupled two-electron Fermi gases of ytterbium atoms*, Phys. Rev. A **94**, 061604 (2016).
- [39] The near-field effect arising from the initial size of the atomic cloud does not significantly affect the measurement of high-momentum tails. An atomic cloud with a radius R after time-of-flight expansion has a near-field effect $dk \simeq Rm/(\hbar t_{tof})$ where t_{tof} is the expansion time. In our experiment, the near-field correction, $dk/k \leq 0.03$, is negligible in the large- k regime ($k > 3k_F$) where the contact is measured.
- [40] Bo Song, Chengdong He, Zejian Ren, Entong Zhao, Jeongwon Lee and Gyu-Boong Jo, *Effective Statistical Fringe Removal Algorithm for High-Sensitivity Imaging of Ultracold Atoms*, Phys. Rev. Applied **14**, 034006 (2020).
- [41] H. Hu, X.-J. Liu and P. D. Drummond, *Universal contact of strongly interacting fermions at finite temperatures*, New Journal of Physics **13**, 035007 (2011).
- [42] M. Sun and X. Leyronas, *High-temperature expansion for interacting fermions*, Phys. Rev. A **92**, 775 (2015).
- [43] T.-L. Ho and E. J. Mueller, *High Temperature Expansion Applied to Fermions near Feshbach Resonance*, Phys. Rev. Lett. **92**, 160404 (2004).
- [44] X.-J. Liu, H. Hu, and P. D. Drummond, *Virial Expansion for a Strongly Correlated Fermi Gas*, Phys. Rev. Lett. **102**, 160401 (2009).
- [45] D. Butts and D. Rokhsar, *Trapped Fermi gases*, Phys. Rev. A **55**, 4346 (1997).
- [46] R. Chang, Q. Bouton, H. Cayla, C. Qu, A. Aspect, C. I. Westbrook and D. Clément, *Momentum-Resolved Observation of Thermal and Quantum Depletion in a Bose Gas*, Phys. Rev. Lett. **117**, 235303 (2016).
- [47] C. Carcy, S. Hoinka, M. G. Lingham, P. Dyke, C. C. N. Kuhn, H. Hu and C. Vale, *Contact and Sum Rules in a Near-Uniform Fermi Gas at Unitarity*, Phys. Rev. Lett. **122**, 203401 (2019).
- [48] S.L. Zhang, M. Y. He, and Qi Zhou, *Contact matrix in dilute quantum systems*, Phys. Rev. A **95**, 062702 (2017).
- [49] S. M. Yoshida, and M. Ueda, *p -wave contact tensor: Universal properties of axisymmetry-broken p -wave Fermi gases*, Phys. Rev. A **94**, 033611 (2016).
- [50] T.L. Ho, and Q. Zhou, *Squeezing out the entropy of fermions in optical lattices*, Proceedings of the National Academy of Sciences, **106**, 6916 (2009).
- [51] T.L. Ho, and Q. Zhou, *Universal Cooling Scheme for Quantum Simulation*, arXiv:0911.5506 (2011).
- [52] A. Mazurenko, C. S. Chiu, G. Ji, M. F. Parsons, M. Kanász-Nagy, R. Schmidt, F. Grusdt, E. Demler, D. Greif and M. Greiner, *A cold-atom Fermi-Hubbard antiferromagnet*, Nature **545**, 462-466 (2017).
- [53] X.-J. Liu, *Virial expansion for a strongly correlated Fermi system and its application to ultracold atomic Fermi gases*, Physics Reports **524**, 37 (2013).
- [54] B. Yang, H. Sun, C.-J. Huang, H.-Y. Wang, Y. Deng, H.-N. Dai, Z.-S. Yuan, and J.-W. Pan, *Cooling and entangling ultracold atoms in optical lattices*, Science **369**, 550 (2020).
- [55] S.-G. Peng, C.-X. Zhang, S. Tan, and K. Jiang, *Contact Theory for Spin-Orbit-Coupled Fermi Gases*, Phys. Rev. Lett. **120**, 060408 (2018).
- [56] P. Zhang and N. Sun, *Universal relations for spin-orbit-coupled Fermi gas near an s -wave resonance*, Phys. Rev. A **97**, 040701(R) (2018).
- [57] J. Jie, R. Qi, and Peng Zhang, *Universal relations of an ultracold Fermi gas with arbitrary spin-orbit coupling*, Phys. Rev. A **97**, 053602 (2018).
- [58] S. E. Gharashi, K. Daily and D. Blume, *Three s -wave-interacting fermions under anisotropic harmonic confinement: Dimensional crossover of energetics and virial coefficients*, Phys. Rev. A **86**, 042702 (2012).
- [59] T. Busch, B. G. Englert, K. Rzazewski, and M. Wilkens, *Two Cold Atoms in a Harmonic Trap - Springer*, Foundations of Physics **28**, 549 (1998).
- [60] E. Marcelino, A. Nicolai, I. Roditi, and A. LeClair, *Virial coefficients for trapped Bose and Fermi gases beyond the unitary limit: An S -matrix approach*, Phys. Rev. A **90**, 053619 (2014).

Acknowledgments

G.-B. J. acknowledges the generous support from the Hong Kong Research Grants Council and the Croucher Foundation through GRF16311516, and GRF16305317, GRF16304918, GRF16306119, C6005-17G, N-HKUST601-17 and the Croucher Innovation grants respectively. Q. Z. is supported by NSF PHY 1806796.